

Accurate Lung Nodules Segmentation with Detailed Representation Transfer and Soft Mask Supervision

Changwei Wang^{1,3}, Rongtao Xu^{1,3}, Shibiao Xu², Weiliang Meng¹,
Jun Xiao³, Qimin Peng⁴, and Xiaopeng Zhang¹

Institute of Automation, Chinese Academy of Sciences¹

Beijing University of Posts and Telecommunications²

University of Chinese Academy of Sciences³

Aksofy (Beijing) Advanced Technology Co., Ltd.⁴

Abstract

Accurate lung nodules segmentation from Computed Tomography (CT) images is crucial to the analysis and diagnosis of lung diseases such as COVID-19 and lung cancer. However, due to the smallness and variety of lung nodules and the lack of high-quality labeling, accurate lung nodule segmentation is still a challenging problem. To address these issues, we propose a complete paradigm for accurate lung nodules segmentation. First, we introduce a new segmentation mask named *Soft Mask* which has richer and more accurate edge details description and better visualization. Correspondingly, we develop a universal semi-automatic *Soft Mask* annotation pipeline to deal with different datasets. Second, a novel **Network** with **Detailed representation transfer** and **Soft Mask supervision (DSNet)** is proposed to process the input low-resolution images of lung nodules into high-quality segmentation results. In our DSNet, we design a novel Selective Detailed Representation Fusion Module to reconstruct the detailed representation to alleviate the small size of lung nodules images. In addition, the adversarial training framework with *Soft Mask* is proposed to further improve the accuracy of segmentation. Extensive experiments validate that our DSNet outperforms the state-of-the-art methods for accurate lung nodules segmentation. And our method also demonstrates competitive results in other accurate medical segmentation tasks. Besides, we provide a new challenging lung nodules segmentation dataset for further studies. [Code release]

Introduction

Since December 2019, the world has been facing a severe health crisis: COVID-19 pandemic (Wang et al. 2020). COVID-19 usually appears as a ground glass opacity (GGO) lung nodule on computed tomography (CT) images (Zhao et al. 2020). In addition, these GGO and other types of lung nodules also potentially contain the risk of lung cancer. Lung cancer is the deadliest type of cancer worldwide for human with a relatively low five-year survival rate of 18% (Siegel, Miller, and Jemal 2019). Accurate segmentation of lung nodule is of great significance for automated

Changwei Wang and Rongtao Xu contributed equally to this work. Shibiao Xu and Weiliang Meng are the corresponding authors (shibiaoxu@hotmail.com; weiliang.meng@ia.ac.cn).

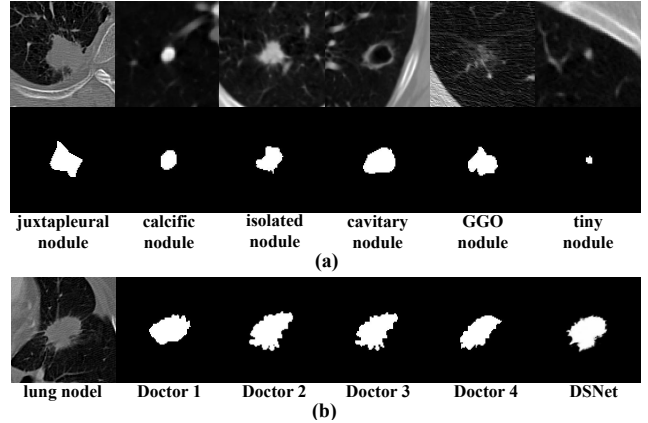


Figure 1: (a): Various types of lung nodules and manual labelings in LIDC. (b): Comparison of the labeling results of four doctors in LIDC with prediction of our proposed DSNet. Our proposed method even achieves better segmentation and visualization results than human radiologists.

disease screening, diagnosis, analysis, and treatment evaluation (MacMahon et al. 2005). However, accurate lung nodule segmentation is still a challenging problem due to the following various reasons.

“One cannot make bricks without straw” is a commonly used expression to imply that it will be difficult to complete the work without the support of the basic conditions. Unfortunately, this tends to be the case for current accurate segmentation of lung nodules without high-quality mask annotations. Obviously, manually labeling lung nodules mask is time-consuming work (Pedrosa et al. 2019). In addition, lung nodules annotation by radiologists is a highly subjective task, often influenced by individual bias and clinical experiences. As shown in Fig. 1 (b), there are obvious differences in the labels of the four doctors. These inconsistencies may cause difficulties in training the segmentation network. The paper (Cai et al. 2018) proposed a semi-automatic mask generation method using the long and short axis of RECIST (Eisenhauer et al. 2009) as weakly supervised information. This method no longer requires the radiologist to manually label the mask but iterative selection. However, the method (Cai et al. 2018) can only get a rough mask

by relying on coarse RECIST marks and GrabCut (Rother, Kolmogorov, and Blake 2004). Therefore, it is difficult for method (Cai et al. 2018) to cope with the task of accurate segmentation of lung nodules with complex edges.

In addition, some inherent characteristics of lung nodules also cause difficulty for its segmentation. Little lung nodules are usually small ($5 \sim 10$ mm) (MacMahon et al. 2005), which leads to the low resolution of the input image. Obviously, low-resolution input loses detailed information of the lesion and makes it difficult to be segmented accurately. Besides, as shown in Fig. 1 (a), lung nodules have significant heterogeneity. Some lung nodules such as GGO and Burr nodules have irregular shapes and complex edges which also pose challenges for accurate segmentation (Lassen et al. 2015). However, as shown in Fig. 1 (b), the existing binary mask cannot describe the edge details of these nodules well, so it is difficult to achieve accurate segmentation and visualization in this case.

To address the above issues, we propose a novel paradigm including a semi-automatic accurate annotation pipeline and a segmentation network (**DSNet**) with detailed representation transfer and *Soft Mask* supervision for accurate lung nodules segmentation. Different from most deep learning based lung nodules segmentation methods (Wang et al. 2017b; Sun, Zheng, and Qian 2017; Liu et al. 2019; Cao et al. 2020), we not only improve the segmentation network architecture, but also recommend that both the input (Low resolution images) and ground-truth (rough binary masks) are also worthy of improvement. Specifically, our proposed *Soft Mask* can preserve rich edge details and smooth transition between lung nodules and surrounding pathological environments. Therefore, the *Soft Mask* has a good visualization effect. And the semi-automatic accurate annotation pipeline we proposed can derive accurate *Soft Masks* from different datasets. In addition, inspired by the recently popular self-supervised pre-training model (He et al. 2020), we carefully designed a Selective Detailed Representation Fusion Module in DSNet to transfer detailed representation knowledge from an off-the-shelf SRGAN (Ledig et al. 2016) model. It can alleviate the problem of the low resolution of the input images. In general, our technical contributions in this work have the following four aspects:

- A new fine mask form *Soft Mask* and the semi-automatic accurate labeling pipeline are proposed to boost segmentation accuracy and obtain excellent visualization.
- We propose a novel DSNet with a Selective Detailed Representation Fusion Module and an Adversarial training framework with *Soft Mask* to convert low-quality images input into high-quality segmentation results.
- Based on the above innovation, a special accurate lung nodules segmentation paradigm is proposed and its performance exceeds state-of-the-art methods on lung nodules segmentation. And it is also suitable for other accurate medical segmentation tasks.
- A new dataset (*LNSM*) is provided, containing 1500 accurate segmentation nodules.

Related Work

Lung Nodules Segmentation and Beyond

Many classic hand-craft feature based methods have been proposed to deal with lung nodules segmentation, such as morphological operations based methods (Kostis et al. 2003), region-growing methods (Kubota et al. 2011b), energy optimization based method (Chan and Vese 2001; Boykov and Kolmogorov 2004), Conditional Random Field (CRF) based method (Wu et al. 2010). However, these methods cannot cope with lung nodules segmentation well (Cao et al. 2020), especially for irregular-shaped nodules.

In recent years, deep learning based methods have gained new attention for medical image analysis and processing. Some convolutional neural networks (CNN) based lung nodules segmentation methods (Wang et al. 2017b; Sun, Zheng, and Qian 2017; Liu et al. 2019; Cao et al. 2020) have achieved highly competitive segmentation accuracy. In addition, some other medical segmentation methods (Ronneberger et al. 2015; Chen et al. 2018; Oktay et al. 2018; Zhou et al. 2018; Gu et al. 2019; Fan et al. 2020) have brought breakthroughs in a variety of medical segmentation tasks. More recently, some transformer-based (Vaswani et al. 2017) models (Valanarasu et al. 2021; Chen et al. 2021) were proposed for medical image segmentation. These methods proposed more complex network architecture to improve the segmentation accuracy, such as the use of attention mechanisms, spatial context, and dense connections. Different from them, our DSNet not only improves the network structure, but also creatively ameliorates the quality and detail of both input images and supervised ground-truth to achieve accurate lung nodules segmentation and impressive visualization.

Soft Labels

Soft labels have been successfully applied to brain lesions segmentation (Kats et al. 2019; Gros, Lemay, and Cohen-Adad 2021). In these works, soft labels are considered to have a better generalization, faster learning speed, and mitigation of network over-confidence. Specifically, Soft labels proposed in the paper (Kats et al. 2019) employed morphological dilation to expand the binary mask and assigned a fixed probability to all pixels within the expanded region. In contrast, the pixels of our proposed *Soft Mask* are not discrete but continuous, so the *Soft Mask* has richer and more accurate edge detail expression. Soft labels proposed in the paper (Gros, Lemay, and Cohen-Adad 2021) is obtained by bilinear interpolation. Since its soft labels are obtained by simple uniform interpolation, it still loses many edge details (such as small burrs around lung nodules). In general, the soft labels proposed in papers (Kats et al. 2019; Gros, Lemay, and Cohen-Adad 2021) softened the binary masks, but they are still rough and difficult to apply to accurate lung nodules segmentation and provide good visualization. By contrast, our proposed *Soft Mask* not only has the advantage of these soft labels but also has an accurate edge representation to reduce the impact of imprecise boundary annotation. In addition, our *Soft Mask* can be obtained from various datasets. In particular, it can use the RECIST marks

in the current hospital picture and archiving systems (PACS) to quickly generate large-scale, high-quality and accurate segmentation masks.

Detailed Representation in Medical images

High-resolution medical images are usually preferred in clinical practice due to more clear image structure and texture details, as well as the benefits to subsequent analysis and processing (Oktay et al. 2016). These detailed representations in high-resolution images are very important for accurate segmentation, especially edge regions. Unfortunately, the extremely small lung nodules are difficult to overcome the challenges of hardware, physical and physiological factors to obtain high-resolution images under the existing imaging system. In recent years, some deep learning based natural images or medical images super-resolution methods (Ledig et al. 2016; Pham et al. 2017; Zhu and Qiu 2021) have excellent performance in image resolution improvement. However, the lack of high-resolution training data limits the application of these methods. In addition, the potential of combining these methods with medical segmentation has not been fully exploited. In this work, we conduct self-supervised training on a super-resolution model for medical images and smartly transfer the detailed representation knowledge in the trained super-resolution model to the lung nodules segmentation pipeline.

Method

In this section, we provide a complete paradigm for accurate lung nodules segmentation. First, we introduce the *Soft Mask* and proposed a pipeline to label it semi-automatically. Then, we present a novel DSNet with Improved Backbone, Selective Detailed Representation Fusion Module and Adversarial training framework with *Soft Mask*.

Soft Mask for Lung Nodules Segmentation

Definition of *Soft Mask*: In most methods, lung nodules are usually labeled and segmented in the form of a binary mask. However, binary masks have many disadvantages in accurately segmenting lung nodules. First, it does not clearly describe the edge and morphological details of the lung nodules, which may cause anatomical information in these marginal regions to be ignored. In addition, the labeling is extremely unbalanced since most of the regions are labeled as non-lesion in the binary mask (Kats et al. 2019), and this imbalance impairs the training of the segmentation network.

To overcome the weakness of the binary mask, inspired by semantic soft segmentation (Aksoy et al. 2018), we introduce a new accurate labeling from the *Soft Mask* of lung nodules. We define every pixel of *Soft Mask* M_i of the i -th pixel as a linear combination of the lesion label L_i and non-lesion background label B_i :

$$M_i = \alpha_i L_i + (1 - \alpha_i) B_i \quad (1)$$

Where the α means the extent of belonging to the lung nodules region. In this work, we employ a close-form-matting algorithm (Levin, Lischinski, and Weiss 2007) to solve the α matrix. close-form-matting converts this problem into a

closed-form solution through linear assumptions and the labeling of known pixels (Trimaps). Therefore, it is important to obtain a high-quality Trimap. We refer the readers to (Levin, Lischinski, and Weiss 2007) for more details.

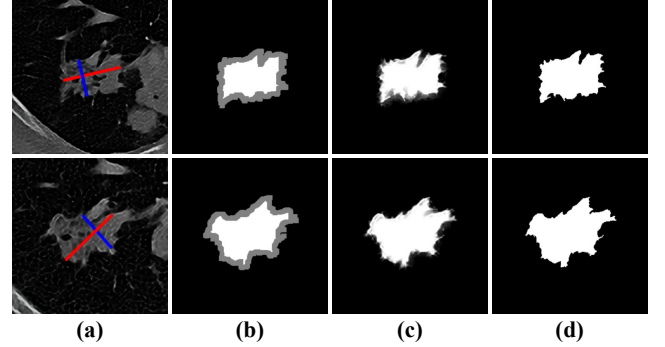


Figure 2: (a) Lung nodules with RECIST marks. The **red line** is the long axis and the **blue line** is the short axis. (b) Trimaps. **White pixels** mean the lesion region. **Black pixels** mean the background region. **Gray pixels** mean the uncertain region. (c) *Soft Masks*. (d) Binarized *Soft Masks*. The *Soft Mask* preserves edge details of lung nodules effectively.

Labeling of *Soft Mask*: In this work, We propose a semi-automatic *Soft Mask* labeling pipeline to deal with priors from different datasets. First, we initialize these different prior information into Trimaps composed of lesion region, background region and the uncertain region as shown in Fig. 2 (b). Specifically, we design the following three strategies for Trimap initialization:

- (1) **Trimaps Generation with normal binary masks:** We use morphological operations to process the binary masks. Specifically, The lesion region is obtained by the erosion operation, the non-lesion background region is obtained by the dilation operation, and the uncertain region is in the middle.
- (2) **Trimaps Generation with binary masks of different doctors:** In order to improve the quality and reliability of labeling, some datasets are repeatedly labeled by different doctors. In LIDC dataset (Armato III et al. 2011), the mask for each lung nodule is marked by four different doctors, as shown in Fig. 1 (b). We set the intersection of these different masks labeled by doctors as the lesion region. And we set the complement of the union of these masks to the background region, and other pixels are uncertain regions.
- (3) **Trimaps Generation with RECIST marks:** Despite their coarseness, RECIST marks (Eisenhauer et al. 2009) are commonly found in current hospital picture and archiving systems (PACS). This means that converting these massive RECIST marks data into accurate masks will have great application value and potential. As shown in Fig. 2 (a), RECIST marks have a long axis and a short axis to mark the diameters of the lesion. First, we use the regions marked on the long axis and the short axis as the prior information of the GrabCut (Rother, Kolmogorov, and Blake 2004) to obtain the initial rough binary masks. Then we apply the morphological processings mentioned in (1) to get the Trimaps.

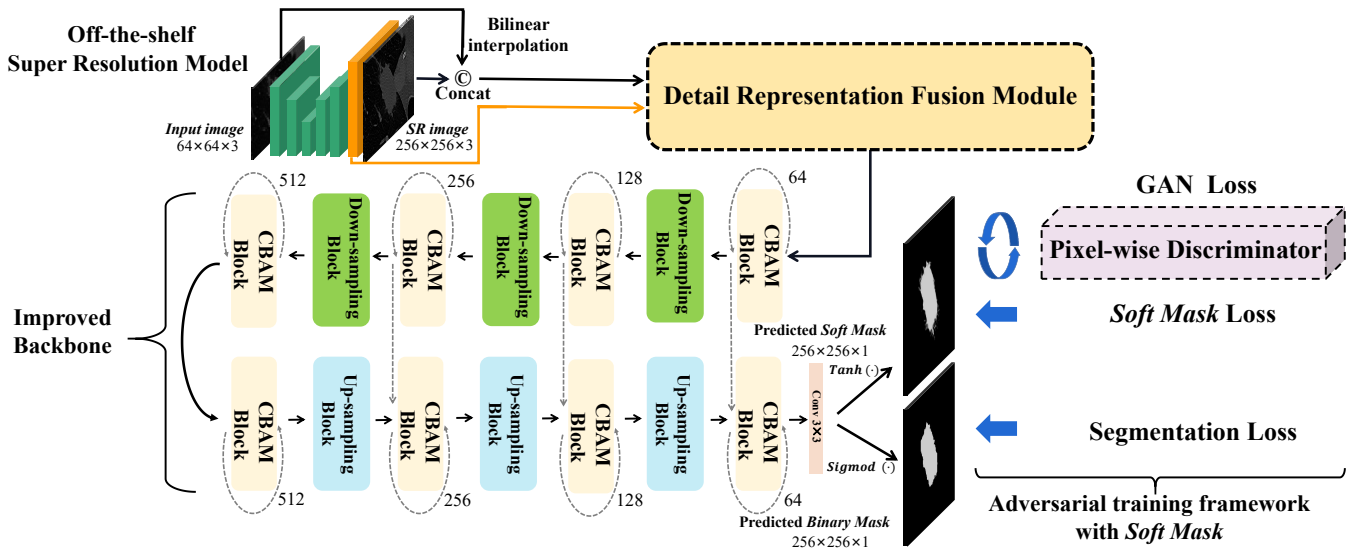


Figure 3: Overview of the proposed DSNet. Our DSNet is composed of Detailed Representation Fusion Module and Improved Backbone and Adversarial training framework with *Soft Mask*.

After getting reliable Trimaps, we use close-form-matting algorithm (Levin, Lischinski, and Weiss 2007) to generate *Soft Masks*, as shown in Fig. 2 (c). As shown in Fig. 2 (d), after the *Soft Mask* is binarized, a accurate binary mask for segmentation can be obtained. Obviously, not all samples that have undergone the above automated processing are high-quality annotations. Therefore, a slight manual selection by doctors is required to ensure the quality of the label. In addition, the entire pipeline is efficient, and it only takes 20 ms (for one 256×256 images: Trimap 5 ms, Close-form-matting 15ms) for us to obtain a high-quality *Soft Mask* label. In this work, we label the lung nodules in the DeepLesion datasets (Yan et al. 2018) with RECIST marks, and form a new dataset containing 1500 lung nodules named *Soft Mask* dataset of Lung Nodules (*LNSM*).

Lung Nodes Segmentation Network with Detailed Representation and Soft Mask (DSNet)

The proposed DSNet that can transform low-quality lung nodules images into a high-quality mask for accurate segmentation is shown in Fig. 3.

Improved Backbone: Based on the classic U-Net (Ronneberger et al. 2015), we improved the backbone to adapt to the accurate segmentation of lung nodules. As shown in Fig. 3, the improved backbone consists of basic blocks, up-sampling blocks and down-sampling blocks. The CBAM block (Woo et al. 2018) is used as the basic block of the backbone. The CBAM block uses both channel attention and spatial attention to enhance the expressive ability of feature maps and thus stimulate the performance of segmentation. In addition, the shortcut connection of ResNet (He et al. 2016) is also used to ensure the propagation of detailed information and gradients. Since the resolution of the input images is usually low, in order to reduce the loss of detail caused by

down-sampling, we use 4×4 convolution with *stride* = 2, *padding* = 1 and Relu as the down-sampling block instead of pooling. The up-sampling block of the decoder consists of 4×4 ConvTranspose and Relu. In addition, the skip connection of U-Net is still used to recover detailed information.

Detailed Representation Transfer: Lung nodules are usually very small ($5 \sim 10$ mm), so common CT systems can only obtain images of lung nodules with low resolution. Low-resolution images mean the loss of detailed information, which is challenging for accurate segmentation of lung nodules with complex shapes and blurred edges. Inspired by the super-resolution methods, we try to reconstruct the detailed information in the high-resolution image and use it to stimulate the performance of accurate segmentation. We will next introduce how to train a super-resolution model without high-resolution lung nodules data and apply the detailed information from the off-the-shelf super-resolution model to the segmentation pipeline.

(1) Self-supervised super-resolution model: The lack of high-resolution lung nodules images makes it difficult to train a super-resolution model. Due to the robustness of the super-resolution methods (Ledig et al. 2016) and the inspiration of the self-supervised pre-training methods (He et al. 2020), we self-supervised train a super-resolution module with a general CT images dataset DeepLesion (Yan et al. 2018). The DeepLesion dataset consists of 32,735 important clinical radiological findings (lesions, tumors, lymph nodes, etc.), so it can be universally adapted to the data of different organs. Specifically, we down-sample the CT images of the Deeplesion dataset from 512×512 to 128×128 for training an SRGAN model (Ledig et al. 2016) (from 128 to 512). Then the trained off-the-shelf super-resolution model is used as a teacher model to transfer the learned detailed knowledge to the Detailed Representation Fusion Module for further lung nodules segmentation.

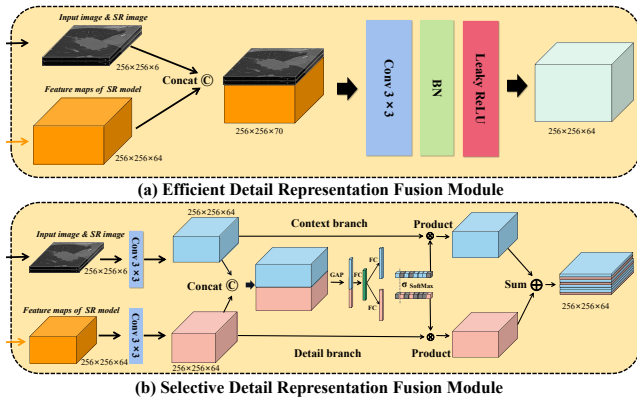


Figure 4: Proposed Detailed Representation Fusion Modules

For transferring the detailed representation into the segmentation pipeline, we designed the following two modules. **(2) Efficient Detailed Representation Fusion Module:** As shown in Fig. 4 (a), we concat the interpolated original image and the super-resolution image, as well as the feature maps output by the last block of the super-resolution model (SR model). The interpolated image retains the original information. Super-resolution image (SR image) and feature maps have rich detailed information. These merged feature maps are then fused by a convolution layer efficiently.

(3) Selective Detailed Representation Fusion Module: Obviously, not all the detailed representations from super-resolution model are conducive to segmentation, and some noise also is introduced. To suppress the noise and better fusion the detailed representation, we further propose a flexible Selective Detailed Representation Fusion Module. Specifically, the context branch extracts feature maps from the super-resolution image and the original image, and the detail branch extracts feature maps from the output feature maps of the super-resolution model, in Fig. 4 (b). Next, we merge the two sets of feature maps and use Global Average Pooling (GAP) and fully connected layers (FC) to learn the corresponding channel weights. Finally, we perform the SoftMax on the channel weights to make the weights play a role in channel selection between the context branch and the detailed branch. After the above operations, Our DSNet learns to adaptively select the detailed representation suitable for segmentation and suppress noise information. Fig. 5 (c) and (d) show the spatial attention maps in the first CBAM block of DSNet. Selective Detailed Representation Fusion Module alleviates the interference of some high-frequency noise.

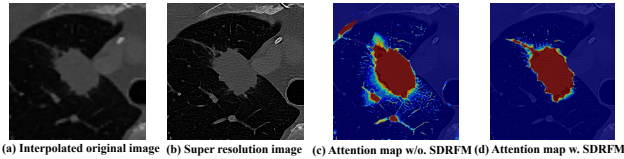


Figure 5: Some visualization samples. SDRFM means Selective Detailed Representation Fusion Module.

Adversarial training framework with *Soft Mask*.

Segmentation Loss is used for the supervision of ground-truth binary masks. We use DICE loss (Milletari et al. 2016) as the segmentation loss:

$$\mathcal{L}_{Seg} = 1 - \frac{2|X_{bin} \cap Y_{bin}|}{|X_{bin}| + |Y_{bin}|} \quad (2)$$

Where X_{bin} and Y_{bin} denote ground-truth binary mask and predicted binary mask respectively, and $|\cdot|$ denotes the number of pixels.

Soft Mask Loss is used to make the predicted *soft mask* has the same distribution as the ground-truth *soft mask*:

$$\mathcal{L}_{Soft} = \|X_{soft} - Y_{soft}\|_{L1} \quad (3)$$

Where X_{soft} and Y_{soft} denote ground-truth soft mask and predicted soft mask respectively, and $\|\cdot\|_{L1}$ denotes the $L1$ distance.

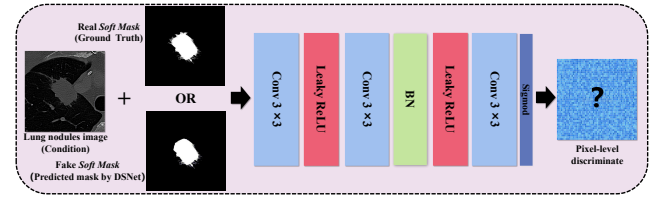


Figure 6: The structure of the pixel-wise Discriminator.

GAN Loss is used to further improve the quality of the predicted *soft mask* by conditional generative adversarial supervision (Mirza and Osindero 2014). As shown in Fig 6, A pixel-wise Discriminator is designed to provide adversarial GAN loss for DSNet. Note that pixel-level discrimination is used here to obtain an accurate pixel-wise adversarial loss. Specifically, the overall objective can be expressed as:

$$G^* = \arg \min_S \max_D \mathcal{L}_{GAN}(S, D), \quad (4)$$

$$\mathcal{L}_{GAN} = \log D(x, y) + \log(1 - D(x, S(x))) \quad (5)$$

Where the DSNet S tries to minimize this objective against an adversarial Discriminator D that tries to maximize it. The x denote lung nodules image (condition), y denote real *soft mask* (ground-truth), and $S(x)$ denote fake soft mask (predicted soft mask). In the training framework, DSNet and the Discriminator have trained alternately.

Implementation

The total loss function of DSNet can be defined as :

$$\mathcal{L}_{total} = \lambda_1 \mathcal{L}_{Seg} + \lambda_2 \mathcal{L}_{Soft} + \lambda_3 \mathcal{L}_{GAN} \quad (6)$$

Where $\lambda_1, \lambda_2, \lambda_3$ are empirically set to 0.5, 100, 1. The Adam optimizer (Kingma and Ba 2014) with poly learning rate policy is used to optimize the network with the training batch size set to 1. The learning rate decays from 0.0002, and the whole training process for *LNSM* dataset typically converges in about 60 epochs and takes about 1.5 hours with a single NVIDIA Titan V GPU. The trained model will be released.

Experiment

In this section, we have conducted thorough experiments on the proposed *LNSM*, LIDC (Armato III et al. 2011), PROMISE (Litjens et al. 2014) and ISBI (Cardona et al. 2010) datasets to verify the effectiveness of our method. Metrics DICE similarity (DICE), sensitivity (SEN) and positive predictive value (PPV) are used to evaluate methods. For convenient, we use the following denotations: TP (true positive), TN (true negative), FP (false positive), FN (false negative). So correspondingly defined as: $DICE = \frac{2 \times TP}{2 \times TP + FP + FN}$; $SEN = \frac{TP}{TP + FN}$; $PPV = \frac{TP}{TP + FP}$.

Accurate lung nodules segmentation

Comparison on our proposed *LNSM*: Lung nodules images with RECIST marks in Deeplesion dataset (Yan et al. 2018) are used to build the proposed *LNSM* dataset. According to the method (strategy (3)) proposed in the previous section, we obtained 1500 cropped 64×64 lung nodules images with *soft masks* and binary masks for training supervision. We randomly divide the dataset into training set (1,000 nodules), test set (400 nodules) and validation set (100 nodules).

Methods	DICE (%)	SEN (%)	PPV (%)
UNet	87.88 ± 1.1	86.62 ± 3.2	89.04 ± 5.7
DeeplabV3+	87.64 ± 2.4	85.21 ± 3.1	88.60 ± 2.4
Attention UNet	87.64 ± 2.4	85.21 ± 1.7	88.60 ± 2.2
UNet++	88.57 ± 2.7	89.24 ± 0.5	91.86 ± 3.7
CENet	89.24 ± 2.2	89.82 ± 1.4	91.33 ± 1.6
UNet3+	90.55 ± 1.5	89.70 ± 2.7	93.65 ± 1.2
INFNet	90.05 ± 1.8	88.17 ± 2.3	93.41 ± 3.7
MedT	90.13 ± 2.6	89.56 ± 3.1	92.41 ± 1.2
DSNet (our)	91.90 ± 1.5	89.97 ± 1.3	94.29 ± 2.5

Table 1: Evaluation results of the *LNSM* dataset.

Table 1 presents a quantitative comparison of some advanced methods on *LNSM* dataset. All methods use the same dataset settings. The outputs are in “mean \pm standard deviation” format. Specifically, UNet (Ronneberger et al. 2015), DeeplabV3+ (Chen et al. 2018), Attention UNet (Oktay et al. 2018), UNet++ (Zhou et al. 2018), CENet (Gu et al. 2019), UNet3+ (Huang et al. 2020), INFNet (Fan et al. 2020) and recent MedT (Valanarasu et al. 2021) are compared and our method significantly exceeds these methods.

Comparison on LIDC: We used a public lung nodules CT dataset from the Lung Image Database Consortium and Image Database Resource Initiative (LIDC) (Armato III et al. 2011) for further comparison. In this study, we studied 986 nodule samples annotated by four radiologists. Due to the differences in labeling between the four radiologists, the 50 % consensus criterion (Kubota et al. 2011a) was used to generate the ground-truth binary masks. We use the method (strategy(2)) of labeling *Soft Mask* mentioned in the previous section to obtain ground-truth *Soft Masks* for training supervision. Then, we randomly partitioned these nodules into three subsets for training, validation, and testing with the number of nodules contained in each subset was 387, 55, and 544, respectively. In addition, we applied K-fold cross-validation of 4-folds during the training process.

We compared our DSNet with some advanced segmentation methods including UNet (Ronneberger et al. 2015), CF-CNN (Wang et al. 2017b), MC-CNN (Shen et al. 2017), MV-DCNN (Wang et al. 2017a), MCROI-CNN (Sun, Zheng, and Qian 2017), Cascaded-CNN (Havaei et al. 2017), DB-ResNet (Cao et al. 2020), which is illustrated in Fig. 2. The result showed that our method outperforms other reported methods in all metrics, especially for DICE and PPV scores.

Methods	DICE (%)	SEN (%)	PPV (%)
UNet	77.84 ± 21.74	77.98 ± 24.52	82.52 ± 21.53
CF-CNN	78.55 ± 12.49	86.01 ± 15.22	75.79 ± 14.73
MC-CNN	75.51 ± 11.4	88.83 ± 12.34	71.42 ± 14.78
MV-DCNN	77.85 ± 12.94	86.96 ± 15.73	77.33 ± 13.26
MCROI-CNN	77.01 ± 12.91	85.43 ± 15.97	73.52 ± 14.62
Cascaded-CNN	79.83 ± 10.91	86.86 ± 13.35	76.14 ± 13.46
DB-ResNet	82.74 ± 10.19	89.35 ± 11.79	79.64 ± 13.54
DSNet (our)	83.35 ± 7.85	89.37 ± 13.24	83.26 ± 14.14

Table 2: Evaluation results of the LIDC dataset.

Ablation study: To justify the effectiveness of proposed modules and strategies, we conduct the following ablation studies on both *LNSM* and LIDC datasets.

Method		<i>LNSM</i>	LIDC
<i>Config.</i>	<i>Variants</i>	<i>DICE (%)</i>	<i>DICE (%)</i>
UNet (Baseline)	<i>orig.</i>	87.88 ± 1.1	77.84 ± 21.74
	+ Improve Backbone	89.57 ± 1.3	79.32 ± 25.34
+ Detailed Representation Transfer	+ SR Input	90.15 ± 2.1	80.69 ± 15.67
	+ EDRFM	90.37 ± 1.9	81.99 ± 17.91
	+ SDRFM	91.03 ± 1.7	82.83 ± 8.15
+ Adversarial training with <i>Soft Mask</i>	+ <i>Soft Mask</i> Loss	91.56 ± 2.4	83.11 ± 11.45
	+ GAN Loss (our DSNet)	91.90 ± 1.5	83.35 ± 7.85

Table 3: Ablation study on the *LNSM* and LIDC benchmarks. We report the *DICE* score for different variants of our DSNet. **DRFM** means Detailed Representation Fusion Module proposed in Section 2. **SR Input** means Using the lung nodules images processed by the super-resolution model as input. **EDRFM** means Efficient Detailed Representation Fusion Module. **SDRFM** means Selective Detailed Representation Fusion Module.

The ablation study is reported in Tab. 3. We use the classic UNet trained with DICE loss as the baseline. After replacing with the improved backbone, the performance is significantly improved, which implies that the network structure is still crucial to lung nodules segmentation. Just using super-resolution images as input, the DICE score has also been slightly improved, indicating that high-resolution images can promote the accurate segmentation of lung nodules. Note that our proposed SDRFM achieves better results than EDRFM, which implies the importance of feature maps selection. Finally, DSNet achieves the best performance after applying a complete Adversarial training with *Soft Mask*.

Robustness study: To further verify the accurate segmentation performance and generalization of our method, we designed an ambitious and challenging experiment: compare our DSNet with human doctors. Specifically, we compare DSNet trained on *LNSM* dataset with four radiologists on LIDC. Note that our DSNet is not retrained, which means that the training set and the test set are cross-domain.

DICE (%)	D1	D2	D3	D4	50% Consensus	DSNet
D1	-	70.65	73.14	62.57	77.51	77.76
D2	70.65	-	74.46	64.91	82.92	74.30
D3	73.14	74.46	-	76.31	83.01	80.88
D4	62.57	64.91	76.31	-	69.74	69.71
50% Consensus	77.51	82.92	83.01	69.74	-	86.35
DSNet	77.76	74.30	80.88	69.71	86.35	-

Table 4: Compare our DSNet with four human doctors on LIDC dataset. D1, D2, D3, D4 mean Doctor 1, Doctor 2, Doctor 3, Doctor 4 respectively. 50 % Consensus means merge at least 50 % of doctors’ labeled regions.

Tab. 4 show the comparison result of our DSNet and human doctors on LIDC. Due to the differences and contradictions in labeling between the four radiologists, the 50 % consensus criterion (Kubota et al. 2011a) is often used as the ground-truth. It can be observed from Tab. 4 that our DSNet, even though it is trained on *LNSM* dataset, is still closer to 50% Consensus than all doctors. On the one hand, the results show that our DSNet has strong robustness and can deal with cross-domain challenges, which implies the potential for clinical application. On the other hand, it shows that the *LNSM* dataset we proposed is also universal and robust. In addition, Fig. 7 shows the visual comparison results between our DSNet and doctors. Our DSNet not only has a higher DICE score, but also has an amazing visualization that even exceeds ground-truth (50 % Consensus). It’s worth mentioning that our visualization results also have been recognized by clinical experts.

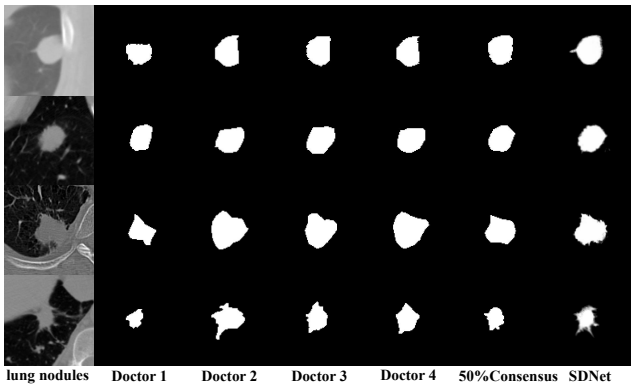


Figure 7: Visual comparison results between our DSNet and doctors.

Accurate other medical images segmentation

To validate our method for the applications of medical images outside of lung nodules, we performed experiments on ISBI (Cardona et al. 2010) and PROMISE (Litjens et al. 2014). The ISBI is a neuronal structure segmentation dataset and the PROMISE is a prostate MRI dataset. After data augmentation, ISBI consists of three subsets: training, verification, and testing (210, 60, 30 samples respectively). And PROMISE consists of three subsets: training, verification, and testing ((460, 65, 130 samples respectively). In addition, we use the *Soft Mask* labeling method (**strategy (1)**) proposed in the previous section to obtain the *Soft Masks* for supervision. We applied 4-folds cross-validation during the training process to cope with the small amount of data. As shown in Tab. 5, Our DSNet achieved the highest DICE and PPV scores and competitive SEN scores on these tasks that also require accurate segmentation. Our DSNet also can be competent for medical segmentation tasks from cells (ISBI) to organs (PROMISE) and shows excellent generalization.

Methods	UNet	UNet3+	INFNet	MedT	DSNet
DICE (%)	93.5 87.9	96.3 91.5	94.5 90.0	93.7 91.4	95.8 92.1
SEN (%)	91.4 88.7	89.9 87.8	92.1 88.6	90.7 89.0	91.3 88.7
PPV (%)	91.3 90.4	94.1 93.3	94.3 92.3	94.4 93.1	94.7 93.6

Table 5: Comparison of methods on ISBI and PROMISE. The **Left** column: Results of ISBI (Cardona et al. 2010). The **Right** column: Results of PROMISE (Litjens et al. 2014).

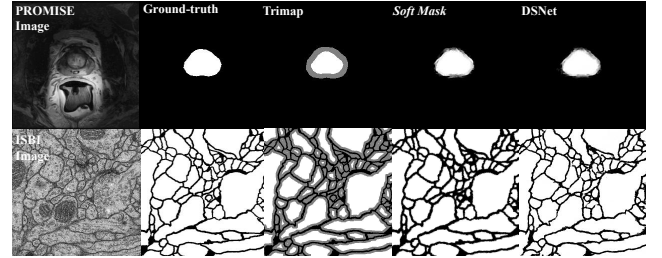


Figure 8: Some visualizations on ISBI and PROMISE. From left to right are the original image, the ground-truth binary mask of the dataset, the Trimap image (Obtained by labeling strategy (1)), the *Soft Mask* and the results of our DSNet prediction.

Conclusion

In this work, we provide a complete solution for accurate lung nodule segmentation, including the *Soft Mask* labeling pipeline and a novel DSNet. In short, we propose a new idea that is not limited to improving the network structure, but to show that the quality of the input image and ground-truth can also be improved. We verify that the proposed method is robust and universally effective on both lung nodule segmentation datasets and other medical datasets. Our method has the great potential to segment other small lesions or small objects accurately while getting an impressive visualization.

References

- Aksoy, Y.; Oh, T.-H.; Paris, S.; Pollefeys, M.; and Matusik, W. 2018. Semantic soft segmentation. *ACM Transactions on Graphics (TOG)* 37(4):1–13.
- Armato III, S. G.; McLennan, G.; Bidaut, L.; McNitt-Gray, M. F.; Meyer, C. R.; Reeves, A. P.; Zhao, B.; Aberle, D. R.; Henschke, C. I.; Hoffman, E. A.; et al. 2011. The lung image database consortium (lidc) and image database resource initiative (idri): a completed reference database of lung nodules on ct scans. *Medical physics* 38(2):915–931.
- Boykov, Y., and Kolmogorov, V. 2004. An experimental comparison of min-cut/max-flow algorithms for energy minimization in vision. *IEEE transactions on pattern analysis and machine intelligence* 26(9):1124–1137.
- Cai, J.; Tang, Y.; Lu, L.; Harrison, A. P.; Yan, K.; Xiao, J.; Yang, L.; and Summers, R. M. 2018. Accurate weakly supervised deep lesion segmentation on ct scans: Self-paced 3d mask generation from recist. *arXiv preprint arXiv:1801.08614*.
- Cao, H.; Liu, H.; Song, E.; Hung, C.-C.; Ma, G.; Xu, X.; Jin, R.; and Lu, J. 2020. Dual-branch residual network for lung nodule segmentation. *Applied Soft Computing* 86:105934.
- Cardona, A.; Saalfeld, S.; Preibisch, S.; Schmid, B.; Cheng, A.; Pulokas, J.; Tomancak, P.; and Hartenstein, V. 2010. An integrated micro-and macroarchitectural analysis of the drosophila brain by computer-assisted serial section electron microscopy. *PLoS Biol* 8(10):e1000502.
- Chan, T. F., and Vese, L. A. 2001. Active contours without edges. *IEEE Transactions on image processing* 10(2):266–277.
- Chen, L.-C.; Zhu, Y.; Papandreou, G.; Schroff, F.; and Adam, H. 2018. Encoder-decoder with atrous separable convolution for semantic image segmentation. In *Proceedings of the European conference on computer vision (ECCV)*, 801–818.
- Chen, J.; Lu, Y.; Yu, Q.; Luo, X.; Adeli, E.; Wang, Y.; Lu, L.; Yuille, A. L.; and Zhou, Y. 2021. Transunet: Transformers make strong encoders for medical image segmentation. *arXiv preprint arXiv:2102.04306*.
- Eisenhauer, E. A.; Therasse, P.; Bogaerts, J.; Schwartz, L. H.; Sargent, D.; Ford, R.; Dancey, J.; Arbut, S.; Gwyther, S.; Mooney, M.; et al. 2009. New response evaluation criteria in solid tumours: revised recist guideline (version 1.1). *European journal of cancer* 45(2):228–247.
- Fan, D.-P.; Zhou, T.; Ji, G.-P.; Zhou, Y.; Chen, G.; Fu, H.; Shen, J.; and Shao, L. 2020. Inf-net: Automatic covid-19 lung infection segmentation from ct images. *IEEE Transactions on Medical Imaging* 39(8):2626–2637.
- Gros, C.; Lemay, A.; and Cohen-Adad, J. 2021. Softseg: Advantages of soft versus binary training for image segmentation. *Medical Image Analysis* 71:102038.
- Gu, Z.; Cheng, J.; Fu, H.; Zhou, K.; Hao, H.; Zhao, Y.; Zhang, T.; Gao, S.; and Liu, J. 2019. Ce-net: Context encoder network for 2d medical image segmentation. *IEEE Transactions on Medical Imaging* 38(10):2281–2292.
- Havaei, M.; Davy, A.; Warde-Farley, D.; Biard, A.; Courville, A.; Bengio, Y.; Pal, C.; Jodoin, P. M.; and Larochelle, H. 2017. Brain tumor segmentation with deep neural networks. *Medical Image Analysis* 35:18–31.
- He, K.; Zhang, X.; Ren, S.; and Sun, J. 2016. Deep residual learning for image recognition. In *Proceedings of the IEEE conference on computer vision and pattern recognition*, 770–778.
- He, K.; Fan, H.; Wu, Y.; Xie, S.; and Girshick, R. 2020. Momentum contrast for unsupervised visual representation learning. In *2020 IEEE/CVF Conference on Computer Vision and Pattern Recognition (CVPR)*.
- Huang, H.; Lin, L.; Tong, R.; Hu, H.; and Wu, J. 2020. Unet 3+: A full-scale connected unet for medical image segmentation. In *ICASSP 2020 - 2020 IEEE International Conference on Acoustics, Speech and Signal Processing (ICASSP)*.
- Kats, E.; Goldberger, J.; Greenspan, H.; ; and and. 2019. Soft labeling by distilling anatomical knowledge for improved ms lesion segmentation. In *2019 IEEE 16th International Symposium on Biomedical Imaging (ISBI 2019)*, 1563–1566. IEEE.
- Kingma, D. P., and Ba, J. 2014. Adam: A method for stochastic optimization. *arXiv preprint arXiv:1412.6980*.
- Kostis, W. J.; Reeves, A. P.; Yankelevitz, D. F.; and Henschke, C. I. 2003. Three-dimensional segmentation and growth-rate estimation of small pulmonary nodules in helical ct images. *IEEE transactions on medical imaging* 22(10):1259–1274.
- Kubota, T.; Jerebko, A. K.; Dewan, M.; Salganicoff, M.; and Krishnan, A. 2011a. Segmentation of pulmonary nodules of various densities with morphological approaches and convexity models. *Medical Image Analysis* 15(1):133–154.
- Kubota, T.; Jerebko, A. K.; Dewan, M.; Salganicoff, M.; and Krishnan, A. 2011b. Segmentation of pulmonary nodules of various densities with morphological approaches and convexity models. *Medical Image Analysis* 15(1):133–154.
- Lassen, B.; Jacobs, C.; Kuhnigk, J.; Van Ginneken, B.; and Van Rikxoort, E. 2015. Robust semi-automatic segmentation of pulmonary subsolid nodules in chest computed tomography scans. *Physics in Medicine & Biology* 60(3):1307.
- Ledig, C.; Theis, L.; Huszar, C.; Caballero, J.; Cunningham, A.; Acosta, A.; Aitken, A.; Tejani, A.; Totz, J.; and Wang, Z. 2016. Photo-realistic single image super-resolution using a generative adversarial network. In *IEEE Computer Society*.
- Levin, A.; Lischinski, D.; and Weiss, Y. 2007. A closed-form solution to natural image matting. *IEEE transactions on pattern analysis and machine intelligence* 30(2):228–242.
- Litjens, G.; Toth, R.; van de Ven, W.; Hoeks, C.; Kerkstra, S.; van Ginneken, B.; Vincent, G.; Guillard, G.; Birbeck, N.; Zhang, J.; et al. 2014. Evaluation of prostate segmentation algorithms for mri: the promise12 challenge. *Medical image analysis* 18(2):359–373.
- Liu, H.; Cao, H.; Song, E.; Ma, G.; and Hung, C. C. 2019.

- A cascaded dual-pathway residual network for lung nodule segmentation in ct images. *Physica Medica* 63:112–121.
- MacMahon, H.; Austin, J. H.; Gamsu, G.; Herold, C. J.; Jett, J. R.; Naidich, D. P.; Patz Jr, E. F.; and Swensen, S. J. 2005. Guidelines for management of small pulmonary nodules detected on ct scans: a statement from the fleischner society. *Radiology* 237(2):395–400.
- Milletari, F.; Navab, N.; Ahmadi, S.-A.; and and. 2016. V-net: Fully convolutional neural networks for volumetric medical image segmentation. In *2016 Fourth International Conference on 3D Vision (3DV)*, 565–571.
- Mirza, M., and Osindero, S. 2014. Conditional generative adversarial nets. *arXiv preprint arXiv:1411.1784*.
- Oktay, O.; Bai, W.; Lee, M.; Guerrero, R.; Kamnitsas, K.; Caballero, J.; de Marvao, A.; Cook, S.; O'Regan, D.; and Rueckert, D. 2016. Multi-input cardiac image super-resolution using convolutional neural networks. In *International conference on medical image computing and computer-assisted intervention*, 246–254. Springer.
- Oktay, O.; Schlemper, J.; Folgoc, L. L.; Lee, M.; Heinrich, M.; Misawa, K.; Mori, K.; McDonagh, S.; Hammerla, N. Y.; Kainz, B.; et al. 2018. Attention u-net: Learning where to look for the pancreas. *arXiv preprint arXiv:1804.03999*.
- Pedrosa, J.; Aresta, G.; Ferreira, C.; Rodrigues, M.; Leitão, P.; Carvalho, A. S.; Rebelo, J.; Negrão, E.; Ramos, I.; Cunha, A.; et al. 2019. Lndb: a lung nodule database on computed tomography. *arXiv preprint arXiv:1911.08434*.
- Pham, C. H.; Ducournau, A.; Fablet, R.; and Rousseau, F. 2017. Brain mri super-resolution using deep 3d convolutional networks. In *IEEE International Symposium on Biomedical Imaging*.
- Ronneberger, O.; Fischer, P.; Brox, T.; ; and and. 2015. U-net: Convolutional networks for biomedical image segmentation. In *International Conference on Medical image computing and computer-assisted intervention*, 234–241. Springer.
- Rother, C.; Kolmogorov, V.; and Blake, A. 2004. " grabcut" interactive foreground extraction using iterated graph cuts. *ACM transactions on graphics (TOG)* 23(3):309–314.
- Shen, W.; Zhou, M.; Yang, F.; Yu, D.; Dong, D.; Yang, C.; Zang, Y.; and Tian, J. 2017. Multi-crop convolutional neural networks for lung nodule malignancy suspiciousness classification. *Pattern Recognit.* 61:663–673.
- Siegel, R. L.; Miller, K. D.; and Jemal, A. 2019. Cancer statistics, 2019. *CA: a cancer journal for clinicians* 69(1):7–34.
- Sun, W.; Zheng, B.; and Qian, W. 2017. Automatic feature learning using multichannel roi based on deep structured algorithms for computerized lung cancer diagnosis. *Computers in Biology and Medicine* 530.
- Valanarasu, J. M. J.; Oza, P.; Hacihaliloglu, I.; and Patel, V. M. 2021. Medical transformer: Gated axial-attention for medical image segmentation. *arXiv preprint arXiv:2102.10662*.
- Vaswani, A.; Shazeer, N.; Parmar, N.; Uszkoreit, J.; Jones, L.; Gomez, A. N.; Kaiser, Ł.; and Polosukhin, I. 2017. Attention is all you need. In *Advances in neural information processing systems*, 5998–6008.
- Wang, S.; Mu, Z.; Gevaert, O.; Tang, Z.; Di, D.; Liu, Z.; and Jie, T. 2017a. A multi-view deep convolutional neural networks for lung nodule segmentation. *Conf Proc IEEE Eng Med Biol Soc* 2017:1752–1755.
- Wang, S.; Zhou, M.; Liu, Z.; Liu, Z.; Gu, D.; Zang, Y.; Dong, D.; Gevaert, O.; and Tian, J. 2017b. Central focused convolutional neural networks: Developing a data-driven model for lung nodule segmentation. *Medical image analysis* 40:172–183.
- Wang, C.; Horby, P. W.; Hayden, F. G.; and Gao, G. F. 2020. A novel coronavirus outbreak of global health concern. *The lancet* 395(10223):470–473.
- Woo, S.; Park, J.; Lee, J.-Y.; and Kweon, I. S. 2018. Cbam: Convolutional block attention module. In *Proceedings of the European conference on computer vision (ECCV)*, 3–19.
- Wu, D.; Lu, L.; Bi, J.; Shinagawa, Y.; Boyer, K.; Krishnan, A.; and Salganicoff, M. 2010. Stratified learning of local anatomical context for lung nodules in ct images. In *2010 IEEE Computer Society Conference on Computer Vision and Pattern Recognition*, 2791–2798. IEEE.
- Yan, K.; Wang, X.; Lu, L.; and Summers, R. M. 2018. DeepLesion: automated mining of large-scale lesion annotations and universal lesion detection with deep learning. *Journal of Medical Imaging* 5(3):1 – 11.
- Zhao, W.; Zhong, Z.; Xie, X.; Yu, Q.; and Liu, J. 2020. Relation between chest ct findings and clinical conditions of coronavirus disease (covid-19) pneumonia: a multicenter study. *American Journal of Roentgenology* 214(5):1072–1077.
- Zhou, Z.; Siddiquee, M. M. R.; Tajbakhsh, N.; and Liang, J. 2018. Unet++: A nested u-net architecture for medical image segmentation. *CoRR* abs/1807.10165.
- Zhu, D., and Qiu, D. 2021. Residual dense network for medical magnetic resonance images super-resolution. *Computer Methods and Programs in Biomedicine*.